

Estimates of hadron azimuthal anisotropy from multiparton interactions in proton-proton collisions at $\sqrt{s} = 14$ TeV

D. d'Enterria^{a,b}, G. Kh. Eyyubova^{c,d}, V. L. Korotkikh^c, I. P. Lokhtin^c, S. V. Petrushanko^c, L. I. Sarycheva^c, A. M. Snigirev^c

^a Laboratory for Nuclear Science, MIT, Cambridge, MA 02139-4307, USA

^b Institut de Ciències del Cosmos & ICREA, Univ. Barcelona, 08028 Barcelona, Catalonia

^c Skobeltsyn Institute of Nuclear Physics, Moscow State University, RU-119991 Moscow, Russia

^d Department of Physics, University of Oslo, PB 1048 Blindern, N-0316 Oslo, Norway

Received: date / Revised version: date

Abstract. We estimate the amount of collective “elliptic flow” expected at mid-rapidity in proton-proton (p - p) collisions at the CERN Large Hadron Collider (LHC), assuming that any possible azimuthal anisotropy of the produced hadrons with respect to the plane of the reaction follows the same overlap-eccentricity and particle-density scalings as found in high-energy heavy ion collisions. Using a Glauber eikonal model, we compute the p - p eccentricities, transverse areas and particle multiplicities for various phenomenological parametrisations of the proton spatial density. For realistic proton transverse profiles, we find integrated elliptic flow v_2 parameters below 3% in p - p collisions at $\sqrt{s} = 14$ TeV.

PACS. 13.85.-t – 13.85.Hd – 25.75.Ld

1 Introduction

With increasing energies, hadronic collisions are characterised by a larger and larger number of produced particles issuing from the fragmentation of a growing number of partons involved in the reaction. In the extreme case of high-energy nucleus-nucleus (A - A) reactions, the multiplicity of released partons is so large – e.g. $\mathcal{O}(1000)$ at midrapidity in central Au - Au collisions at RHIC energies ($\sqrt{s_{NN}} = 200$ GeV) – that they interact strongly among each other leading to “hydrodynamical flow” behaviours [1]. A distinct consequence of such partonic expansion effects is an azimuthal anisotropy of the final particles produced, $dN/d\Delta\phi$, with respect to the reaction plane¹, $\Delta\phi = \phi - \Phi_{RP}$. At RHIC energies, the large “elliptical” anisotropy measured in the data has provided detailed information on the degree of collectivity reached in the early stages of nuclear collisions (see e.g. [2] for a recent comprehensive review).

The parton density inside hadrons grows very rapidly with increasing energies, as more and more gluons share smaller and smaller fractional momenta $x \equiv p_{parton}/p_{hadron}$ (see e.g. [3, 4] and refs. therein). Thus, at high enough energies the proton itself can be considered as a *dense* and *extended* partonic object, and proton-proton collisions can be viewed very much like collisions of “light nuclei” composed of their constituent gluons. The possibility of having multiple parton interactions

(MPI) happening simultaneously at different impact parameters in hadronic collisions has been discussed since long in the literature [5]. Signals of multiple parton scatterings have been observed experimentally in p - \bar{p} collisions at centre-of-mass (c.m.) energies $\mathcal{O}(1$ TeV) in charged particle multiplicity distributions [6] as well as in multi-jets events [7–9]. At LHC energies, recent developments of general-purpose Monte Carlo (MC) event generators such as PYTHIA [10] and HERWIG [11] include an impact-parameter-space description of the p - p collision to account for MPI effects. As a result of the large number of low- x gluons and increasing multi-parton collisions, the MC predictions for the *total* number of produced particles in “central” p - p collisions at $\sqrt{s} = 14$ TeV, are pretty large – up to five hundreds hadrons – similar to those measured e.g. in intermediate-size nuclear (Cu - Cu) reactions at $\sqrt{s_{NN}} = 200$ GeV [12] where a significant elliptic flow has been observed in the data [13]. Given this situation, it does not seem unjustified to contemplate the possibility of having some type “collective” behaviour also in the final-state of proton-proton collisions at LHC energies [14].

In this paper, we explore the possibility of observing genuine collective expansion effects, such as an azimuthal anisotropy with respect to the plane of the reaction, in p - p collisions at $\sqrt{s} = 14$ TeV. We note that the partons involved in the scatterings of relevance for such collective effects have rather moderate virtualities of the order of the average transverse momentum expected in a minimum-bias p - p collision at the LHC, i.e. $\mathcal{O}(0.7$ GeV). Recent attempts to estimate similar effects

¹ The reaction plane of a collision is spanned by the vector of the impact parameter b between the centers of the two colliding objects, and the beam direction. Its azimuth is given by Φ_{RP} .

have been considered in the context of percolation [15], colour-dipole saturation² [16] and (viscous) hydrodynamics [17] models. In our work, we take a more empirical (i.e. less model-dependent) approach and we simply assume that the eccentricity and multiplicity dependence of the elliptic flow experimentally observed in high-energy heavy ion collisions (Section 2) holds also for proton collisions at the LHC. Using a geometrical eikonal approach (Section 3), we determine the eccentricity of the transverse overlap region in p - p collisions for different proposed proton spatial densities (Section 4), and then we estimate the resulting associated azimuthal anisotropy for various impact-parameters (Section 5).

2 Elliptic flow scaling in ultrarelativistic heavy ion collisions

One of the main results at RHIC is the observation [18, 19] of a large harmonic modulation of the azimuthal distribution of the produced hadrons, $dN/d\Delta\phi$, with respect to the reaction-plane in A - A collisions with non-zero impact parameter, i.e. with a lens-shaped overlap zone between the colliding nuclei. The measured preferential “in-plane” emission is consistent with an efficient translation of the initial coordinate-space anisotropy into a final “elliptical” asymmetry in momentum-space through rescatterings between the produced partons in the early stages of the collision [20, 21]. The strength of the elliptic flow asymmetry in A - A collisions is quantified via the second Fourier coefficient $v_2 \equiv \langle \cos(2\Delta\phi) \rangle$ of the azimuthal decomposition of the single inclusive hadron spectrum with respect to the reaction plane [22, 23]

$$E \frac{d^3N}{d^3p} = \frac{1}{2\pi} \frac{d^2N}{p_T dp_T dy} \left(1 + 2 \sum_{n=1}^{\infty} v_n \cos[n(\phi - \Phi_{RP})] \right). \quad (1)$$

The large integrated³ $v_2 \approx 0.06$ measured in Au - Au collisions at $\sqrt{s_{NN}} = 200$ GeV [18, 19] is well reproduced by hydrodynamical simulations [20, 21] that predict the development of collective motion along the pressure gradient of the system, which is larger for the in-plane directions parallel to the smallest dimension of the lens-shaped overlap zone. Within this scenario, one naturally expects v_2 to be directly proportional to (i) the *density* of produced particles in the transverse plane, as well as to (ii) the original spatial anisotropy of the system quantified by its *eccentricity*, usually defined as $\epsilon = \langle y^2 - x^2 \rangle / \langle x^2 + y^2 \rangle$ (where x, y are the transverse dimensions of the “lens”, and the average is taken over the initial nuclear profile with some weight, see later) [24, 25].

Experimental heavy ion data at different c.m. energies with different colliding systems and varying centralities [26] indeed

² Strictly speaking, the origin of elliptic flow in this work is of a different nature (initial parton distributions) than the final-state collective effects of interest here.

³ The v_2 coefficient is a function of rapidity and transverse momentum, and as such it is often referred to as *differential* flow. Hereafter, we will be interested in *integrated* flow, namely the value of the v_2 coefficient averaged over transverse momentum and rapidity in a given event.

indicate a proportionality of the v_2/ϵ ratio with the particle multiplicity normalised by the size of the system, i.e. $v_2/\epsilon \propto (dN/dy)/A_\perp$, where dN/dy is the total hadron multiplicity⁴ N per unit rapidity y , and the overlap transverse area A_\perp is calculated via a Glauber geometrical model (see e.g. [27]) with standard Woods-Saxon distributions for the initial nuclear distributions [28]. An attempt to parameterise the observed v_2/ϵ dependence on particle density based on an “incomplete equilibration” model has been developed in Refs. [29, 30] in terms of the *Knudsen number* $K = \lambda/R$, where λ is the mean free path of the interacting partons and R a typical length scale (e.g. the radius) of the system. By definition, K^{-1} is the mean number of collisions per particle (i.e. the medium *opacity*), and the ideal hydrodynamics limit corresponds to $K \rightarrow 0$. Since $\lambda = 1/(\sigma_{gg}\rho)$, where σ_{gg} is the effective parton-parton (mostly gluon-gluon) cross section, and since $\rho(\tau) = 1/(\tau A_\perp) \cdot dN/dy$ is the (time-dependent) density of the medium, for a typical time $\tau = R/c_s$ (where c_s is the medium speed of sound) one can write the (inverse of the) Knudsen number as

$$K^{-1} = \frac{\sigma_{gg} c_s}{A_\perp} \frac{dN}{dy}, \quad (2)$$

Within this model, the dependence of v_2/ϵ on dN/dy in A - A collisions can be obtained with the simple expression [30]:

$$\left(\frac{v_2}{\epsilon} \right) = \left(\frac{v_2^{hydro}}{\epsilon} \right) \frac{1}{(1 + K/K_0)}, \quad (3)$$

where K is given by Eq. (2) and $K_0 \approx 0.7$ is obtained from a transport model calculation [31]. Thus, taking $c_s = 1/\sqrt{3}$ for the speed of sound of an ideal parton gas, the model has just two free parameters to fit to the data: the effective partonic cross section σ_{gg} and the elliptic flow in the hydrodynamic-limit v_2^{hydro} . A good agreement with Au - Au and Cu - Cu data at RHIC is obtained with $\sigma_{gg} = 5.5$ mb and $(v_2^{hydro}/\epsilon) = 0.22$ [30] for a spatial density of the colliding nuclei (needed to determine ϵ and A_\perp) based on Color Glass Condensate (CGC) initial conditions⁵ [32]. Namely, the elliptic flow data can be well reproduced with the following numerical expression

$$\begin{aligned} \left(\frac{v_2}{\epsilon} \right) &= \left(\frac{v_2^{hydro}}{\epsilon} \right) \left(\frac{1}{K_0 \sigma_{gg} c_s} + \frac{dN}{dy} \frac{1}{A_\perp} \right)^{-1} \cdot \frac{dN}{dy} \frac{1}{A_\perp} \\ &= 0.22 \cdot \left(0.45 + \frac{dN}{dy} \frac{1}{A_\perp [\text{mb}]} \right)^{-1} \cdot \frac{dN}{dy} \frac{1}{A_\perp [\text{mb}]}. \end{aligned} \quad (4)$$

In this paper we take as basic assumption that the parton medium produced in the overlap region of p - p collisions at LHC energies has similar hydrodynamic properties as that in A - A collisions at RHIC and, thus, that the resulting anisotropic

⁴ Hereafter, dN/dy represents the particle multiplicity per unit-rapidity *at midrapidity*, i.e. $dN/dy|_{y=0}$, but for simplicity we omit the subindex.

⁵ We note that Eq. (4) is a “conservative” estimate of the magnitude of v_2/ϵ since the alternative initial Glauber matter distribution – with fit parameters $\sigma_{gg} = 4.3$ mb and $(v_2^{hydro}/\epsilon) = 0.30$ – results in a 8%–20% larger v_2/ϵ ratio.

flow parameter v_2 follows the same eccentricity and “transverse” multiplicity scalings given by Eqs. (2) and (3). For simplicity we will use the same fit-parameters for σ_{gg} and (v_2^{hydro}/ϵ) obtained in [30], i.e. we will assume that Eq. (4) holds too for p - p at the LHC. From the eccentricity ϵ , transverse overlap area A_\perp and hadron multiplicity dN/dy in p - p collisions, determined from a Glauber eikonal model using different phenomenological parametrisations of the proton spatial density distribution, we can thus estimate the expected elliptic flow parameter, v_2 , as a function of the p - p “centrality” or impact parameter b .

3 Eikonal model for proton-proton collisions

The standard procedure to determine the transverse overlap area, eccentricity and final multiplicities in the collision of two nuclei separated by impact parameter b is based on a simple Glauber multi-scattering eikonal model that assumes straight-line trajectories of the colliding nucleus constituents. A recent review that describes the basic formalism can be found in [27]. Often, experimentally it is more useful to introduce the “reaction centrality” C as a proxy for the impact-parameter b of a given collision, by dividing the particle production cross section into centrality bins $C_k = C_1, C_2, \dots$ according to some fractional interval ΔC of the total cross section, e.g. $\Delta C = 0.0 - 0.1$ represents the 10% most central collisions. A convenient geometrical definition of centrality is $C = b^2/(4R^2)$, as it corresponds to percentiles of the total inelastic cross section in the case of two colliding black disks (or any other distribution with small diffuseness) with the same radii R , see Appendix I for details.

Thickness and overlap functions, number of binary parton-parton collisions: The basic quantity of interest in a Glauber approach is the *thickness* (or *profile*) *function* of the collision which in the case of a nuclear reaction gives the density of nucleons ρ per unit area $dx dy$ along the direction z separated from the center of the nucleus by an impact parameter b , i.e. $T_A(x, y) = A \int dz \rho(x, y, z)$ for a nucleus of mass number A . By analogy to the nuclear case, the thickness function of a proton with N_g partons can be written as

$$T_p(x, y) = N_g \int dz \rho(x, y, z), \quad (5)$$

normalised to $\int d^2b T_p(b) = N_g$.

The *overlap function* of a proton-proton collision at b can be obtained as a convolution over the corresponding thickness functions of each proton

$$T_{pp}(b) = \int dx dy T_{p,1}(x + b/2, y) T_{p,2}(x - b/2, y), \quad (6)$$

normalised to $\int d^2b T_{pp}(b) = N_g^2$.

For a given parton-parton cross section σ_{gg} , we can then define the number of binary parton-parton collisions in a p - p collision

at a given impact parameter b

$$N_{coll,gg}(x, y; b) = \sigma_{gg} T_{p,1}(x + b/2, y) T_{p,2}(x - b/2, y),$$

$$N_{coll,gg}(b) = \int dx dy N_{coll,gg}(x, y; b) = \sigma_{gg} T_{pp}(b). \quad (7)$$

Finally, the probability density of an inelastic parton-parton interaction at impact parameter b can be defined as

$$\frac{d^2 P_{gg}^{inel}}{d^2b}(b) = \frac{1 - e^{-\sigma_{gg} T_{pp}(b)}}{\int d^2b (1 - e^{-\sigma_{gg} T_{pp}(b)})}, \quad \text{or}$$

$$\frac{d P_{gg}^{inel}}{db}(b) = 2\pi b \frac{1 - e^{-\sigma_{gg} T_{pp}(b)}}{\int d^2b (1 - e^{-\sigma_{gg} T_{pp}(b)})}, \quad (8)$$

according to Poisson statistics. Note that the denominator – which sums over all events with at least one parton-parton interaction – is just the total inelastic p - p cross section σ_{pp}^{inel} .

Eccentricity and overlap area: The eccentricity of a p - p collision at impact parameter b can be obtained from the asymmetry ratio between the x and y “semi-axis” dimensions of the overlap zone, weighted by the number of parton-parton collisions at b :

$$\epsilon(b) = \frac{\langle y^2 - x^2 \rangle}{\langle y^2 + x^2 \rangle} = \frac{\int dx dy (y^2 - x^2) N_{coll,gg}(x, y; b)}{\int dx dy (y^2 + x^2) N_{coll,gg}(x, y; b)}, \quad (9)$$

Other weights are possible too, see [2], but we take $N_{coll,gg}(b)$ as a natural choice – also used in more sophisticated hydrodynamics approaches [33] – since our picture for LHC energies is based on parton-parton collisions⁶. As a cross-check, we tested also a weight based on the number of participating gluons, obtained from $T_p(x, y)$ as described in [34], obtaining similar results for $\epsilon(b)$ for various proton densities.

The effective transverse overlap area between the two protons is defined as in [30]:

$$A_\perp(b) = 4\pi \sqrt{\langle x^2 \rangle} \sqrt{\langle y^2 \rangle}, \quad (10)$$

where the weighted averages are the same as in Eq. (9). We note that there is no commonly accepted definition of the absolute normalisation of the overlap area. Our area definition with maximum magnitude 4π , is four times larger than that defined in [23] but coincides practically with the geometrical overlap area of two disks with uniform two-dimensional distribution of density.

Hadron multiplicity: In heavy ion collisions, the centrality dependence of the final hadron multiplicity density is found to

⁶ Our eccentricity definition, Eq. (9), and the incomplete thermalisation model one [30] are mathematically identical (modulo, a sign) in the case $\langle x \rangle = \langle y \rangle = \langle xy \rangle = 0$, since our spatial densities depend only on $r = \sqrt{x^2 + y^2}$ and the $N_{coll,gg}(x, y)$ weight is an even function of x and y .

depend on a combination of the number of nucleon binary collisions and “participant” pairs [1]. Since, at LHC energies, fragmentation of *mini*-jets produced in *semi*-hard parton-parton scatterings is the largest contribution to midrapidity particle production, we will consider as a plausible operational assumption that the final particle multiplicity in a proton-proton collision follows the same impact-parameter-dependence as that of the number of binary parton-parton collisions $N_{coll,gg}(b)$, i.e. that

$$\frac{dN}{dy}(b) = \frac{dN_0}{dy} \cdot N_{coll,gg}(b), \quad (11)$$

where the absolute normalisation dN_0/dy is chosen so as to reproduce the *minimum-bias* p - p multiplicity, namely the average multiplicity in a proton-proton collision integrated over all impact-parameters

$$\frac{dN_{MB}}{dy} = \frac{dN_0}{dy} \int d^2b N_{coll,gg}(b) \frac{d^2 P_{gg}^{inel}}{d^2b}(b), \quad (12)$$

which, at midrapidity at LHC energies, is expected to be $dN_{MB}/dy \approx 10$ according to the PYTHIA [10] or PHOJET [35] MCs based on various extrapolations from lower energy data.

3.1 Proton spatial transverse densities

The matter distribution in transverse space of the colliding protons, $\rho(x, y)$ determines the probability to have a given number of parton-parton interactions at impact parameter b . In order to quantify the proton profile function, Eq. (6), one often assumes a spherically symmetric distribution of matter in the Breit system, $\rho(x)d^3x = \rho(r)d^3x$, and, for simplicity, one takes the same spatial distribution for all parton species in the proton (valence and sea quarks, gluons) and momenta, and neglects any correlations among them. The spatial proton density has been parameterised with different distributions in the literature (see e.g. [8, 10]) such as:

- *Hard sphere*: The simplest model is to consider that the proton has a spherical form with uniform parton density of radius R :

$$\rho(r) = \frac{1}{4/3 \pi R^3} \Theta(r - R) \quad (13)$$

The associated root-mean-square (*rms*) charge radius is $R_{rms} = \sqrt{\langle r^2 \rangle} = \sqrt{3/5} R$. Of course this is an unrealistic approximation of the proton shape⁷, but we keep it as an “extreme” case since the overlap area of two such distributions has very large eccentricities.

- *Exponential*: Matter can be distributed in the proton according to its *charge form factor*, which is well represented by an exponential expression in coordinate space:

$$\rho(r) = \frac{1}{8\pi R^3} e^{-r/R}, \quad (14)$$

reproducing to a large extent the spatial distribution of the *valence* quarks, with *rms* radius $R_{rms} = \sqrt{12} R$.

⁷ E.g. in particular at higher virtualities, such a profile violently disagrees with the small- t (where t is the squared momentum exchanged) J/ψ data at HERA [36].

- *Fermi distribution*: The standard spatial density for nuclei is the Fermi-Dirac (or Woods-Saxon) distribution with radius R and surface thickness a

$$\rho(r) = \frac{\rho_0}{e^{(r-R)/a} + 1}, \quad (15)$$

where ρ_0 is a normalisation constant so that $\int d^3r \rho(r) = 1$. The associated *rms* radius is $R_{rms} = \sqrt{3/5} R$ in the limit $a/R \rightarrow 0$ and $R_{rms} = \sqrt{12} a$ for $a/R \rightarrow \infty$. For $a/R = 0.2$, $R_{rms} \approx 1.07 R$.

- *Gaussian*: A simple Gaussian ansatz, although not very realistic, makes the subsequent calculations especially transparent and, therefore, is often used in the literature:

$$\rho(r) = \frac{1}{(\sqrt{2\pi} R)^3} \exp\left\{-\frac{r^2}{2R^2}\right\}. \quad (16)$$

The corresponding *rms* radius is given by $R_{rms} = \sqrt{3} R$.

- *Double-Gaussian*: This corresponds to a distribution with a small core region of radius a_2 containing a fraction β of the total hadronic matter, embedded in a larger region of radius a_1 :

$$\rho(r) \propto \frac{1-\beta}{a_1^3} \exp\left\{-\frac{r^2}{a_1^2}\right\} + \frac{\beta}{a_2^3} \exp\left\{-\frac{r^2}{a_2^2}\right\}. \quad (17)$$

Although the Gaussian and double-Gaussian are popular proton density choices (e.g. in the PYTHIA MC), we will not consider them hereafter because mathematically the convolution of two such distributions results respectively in an exactly null or very small eccentricity, i.e. they cannot generate any elliptic flow according to our ansatz, Eq. (4).

Table 1 lists the input parameters used for three of the five proton densities mentioned above. The chosen radius R of the hard-sphere parametrisation is consistent with electron-proton scattering fits [37] and with diffractive results at HERA (more sensitive to the *gluon* density) [38]. The parameters of the exponential (R) and Fermi-I (R and a) distributions are those obtained by the CDF collaboration in their data analysis of double parton scatterings in p - \bar{p} collisions at $\sqrt{s} = 1.8$ TeV [8]. In addition, we quote the parameters of the proton Fermi-II distribution obtained from a Fourier transformation of the energy-dependent p - p elastic amplitude as discussed in [39]. Such an approach aims at taking into account the effective growth of the proton size due to the larger transverse spread (“diffusion”) of partons in the proton for increasing collision energy. Within this framework, the radius of the strong interactions is expected to be a factor 1.5 larger at the LHC compared to fixed-target energies. From unitarity (i.e. the optical theorem), the squared c.m. energy (s) dependence of the inelastic (total minus elastic) p - p cross section can be written as an integral over impact parameters [40]:

$$\sigma_{pp}^{inel}(s) = \sigma_{pp}^{tot}(s) - \sigma_{pp}^{el}(s) = \int d^2b [2\text{Re} \Gamma_{pp}(s; b) - |\Gamma_{pp}(s; b)|^2], \quad (18)$$

where $\Gamma_{pp}(s; b)$ is the profile function of the elastic amplitude and the integrand represents the distribution of the cross section

Table 1. Top rows: Radius R and diffusivity a parameters for various proton spatial densities, Eqs. (13) – (15), and effective number of gluons N_g in the proton, considered in this work. The three bottom rows show the maximum eccentricity and overlap area and inelastic cross section derived for p - p collisions at $\sqrt{s} = 14$ TeV from each set of parameters within our Glauber approach. The last column shows the corresponding values for typical Au - Au collisions at RHIC energies.

	Hard sphere refs. [37, 38]	Exponential ref. [8]	Fermi-I ref. [8]	Fermi-II ref. [39]	Fermi Au - Au ref. [28]
radius R (fm)	0.89	0.20	0.56	1.05	6.36
diffusivity a (fm)	–	–	0.112	0.29	0.54
effective number of partons N_g	17	9	17	4	197 (nucleons)
rms radius R_{rms} (fm)	0.69	0.70	0.60	1.34	5.32
diffusivity/radius a/R	–	–	0.2	0.28	0.085
effective partons/fm ³ $N_g \rho(r = 0 \text{ fm})$	5.8	44.8	16.7	0.48	0.17 (nucleons/fm ³)
p - p eccentricity ϵ_{max} at $b \approx 2R_{rms}$	1.	-0.4	0.07	-0.05	0.4
p - p overlap area A_{\perp} at $b = 0$ fm (fm ²)	1.6	0.58	0.85	3.8	85.
p - p inelastic cross section σ_{pp}^{inel} (mb)	80.	79.6	78.5	90.	7110

for generic inelastic collisions (i.e., summed over all inelastic final states) over impact parameters. The s -dependence of the inelastic probability defined as

$$\frac{d^2 P_{gg}^{inel}}{d^2 b}(b) = P_{pp}^{inel}(s; b) = \frac{2\text{Re } \Gamma_{pp}(s; b) - |\Gamma_{pp}(s; b)|^2}{\sigma_{pp}^{inel}(s)}. \quad (19)$$

can be fitted to the available p - p elastic data at high-energies [41] and extrapolated [39] to LHC energies⁸. By fitting $P_{gg}^{inel}(s; b)$ to Eq. (15), we obtain the R and a parameters for the Fermi-II spatial density quoted in Table 1.

For each one of the density parametrisations considered, we obtain a proton root-mean square (rms) charge radius not far from that obtained from the world-data on e - p elastic scattering at low momentum transfer ($Q < 4 \text{ fm}^{-1}$): $R_{rms} \approx 0.89 \text{ fm}$ [42], except for the Fermi-II case which, as aforementioned, yields an effective proton radius twice larger at the LHC than observed at low energies. For comparison purposes with p - p , we add also in the last column of Table 1 the results for Au - Au collisions at $\sqrt{s_{NN}} = 200 \text{ GeV}$ with the standard Au Fermi distribution parameters [28].

The parton-number normalisation N_g of the proton thickness function, Eq. (6), can be obtained by requiring that the proton-proton inelastic cross section obtained from the p - p overlap function, Eq. (7), in the eikonal approximation

$$\sigma_{pp}^{inel} = \int d^2 b \left(1 - e^{-\sigma_{gg} T_{pp}(b)} \right) \quad (20)$$

⁸ We note that the parton-parton cross section, $\sigma_{gg} = 7.8 \text{ mb}$, obtained from the fit of [39] is not far from the $\sigma_{gg} = 5.5 \text{ mb}$ obtained within the incomplete thermalisation model, Eq. (4). Both should be interpreted as *effective* semihard partonic cross-sections, larger than the standard perturbative gluon-gluon cross-section which at LO is $\sigma_{gg} = 9/2 \pi \alpha_s^2 / \mu^2 \approx 2 \text{ mb}$ for $\alpha_s = 0.5$ at a p_T -cutoff of order $\mu = 1 \text{ GeV}$.

is in the range expected at LHC energies, $\sigma_{pp}^{inel} \approx 80 \text{ mb}$ [10, 35], for our considered effective parton-parton cross section of $\sigma_{gg} = 5.5 \text{ mb}$. The corresponding number of partons normalisation N_g is shown in the Table 1 for each proton matter distribution. We also tabulate the product $N_g \rho(r = 0 \text{ fm})$ indicating the parton density in the centre of the proton. For comparison, we also show the density in the center of the Au nucleus (with $A = 197$ nucleons), which is equal to the well-known value $A \rho_A(r = 0 \text{ fm}) = 0.17 \text{ nucleon/fm}^3$. The corresponding inelastic Au - Au cross section at $\sqrt{s_{NN}} = 200 \text{ GeV}$, $\sigma_{AuAu} = 7110 \text{ mb}$, obtained from Eq. (20) with $\sigma_{NN} = 42 \text{ mb}$, is larger as expected than that of two black absorptive hard disks, $\sigma_{AuAu} = 5080 \text{ mb}$, as the Fermi profile for both nuclei has long tails.

3.2 Number of binary collisions and parton-parton inelastic probability

In any eikonal approach, once the spatial densities of the two colliding objects are known, one can derive any geometrical quantity related to their interaction from the overlap function, Eq. (7), or equivalently from the number of binary collisions of their constituent particles, Eq. (7). In the p - p case, the number of parton-parton collisions $N_{coll,gg}$ as a function of scaled impact parameter⁹ $b/2R$ and centrality $C = b^2/(4R^2)$ for the different proton spatial densities considered in this work are shown in the left and right plots of Figure 1, respectively. The plot as a function of centrality is shown as an histogram with binning $\Delta C = 0.2$ as could be obtained experimentally by dividing the data in 20% fractions of the measured cross section (e.g. based on an observable monotonically increasing with impact parameter, such as the event particle multiplicity).

The exponential and Fermi distributions feature a long tail well beyond twice the radii R , whereas the hard-sphere parametrisation dives off quickly when b approaches $2R$. For the most

⁹ For the exponential density, for which R and R_{rms} are quite different, we use $b/(2R_{rms})$.

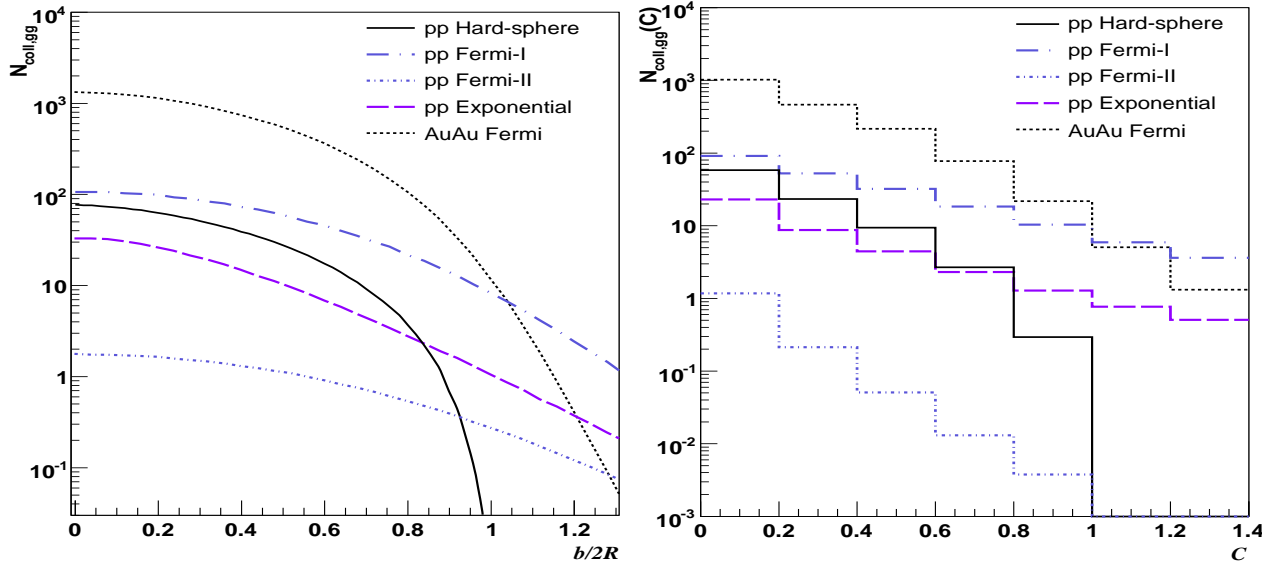


Fig. 1. Number of binary parton-parton collisions in p - p collisions at $\sqrt{s} = 14$ TeV as a function of scaled impact parameter $b/2R$ (left) and centrality C (right) for the different proton density distributions considered in this work (Table 1). For comparison, the results for Au - Au at RHIC energies are shown as a dotted line.

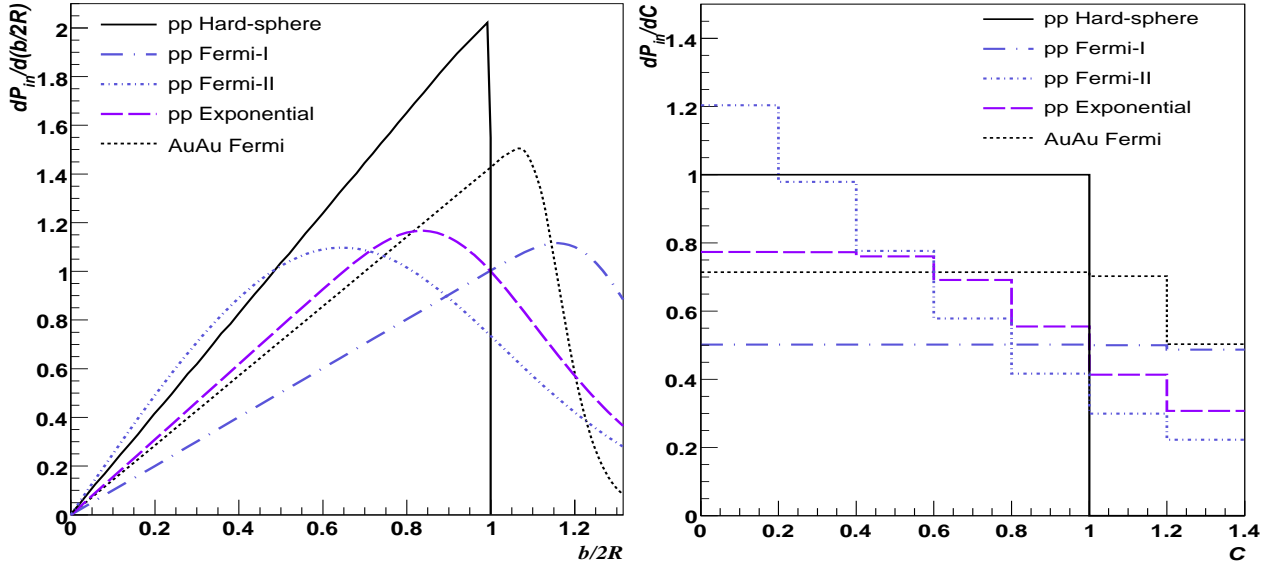


Fig. 2. Probability density (normalised to unity) of inelastic parton scatterings in p - p collisions at $\sqrt{s} = 14$ TeV as a function of scaled impact parameter $b/2R$ (left) and centrality C (right) for the different proton density distributions considered in this work (Table 1). For comparison, the results for Au - Au at RHIC energies are shown as a dotted line.

central p - p collisions ($b = 0$ fm), the hard-sphere and Fermi-I distributions yield about 100 parton-parton interactions, the exponential gives about 30 collisions, and the Fermi-II distribution, which has a larger proton size and thus a more “dilute” parton density, just 2 collisions. For comparison, the number of nucleon-nucleon collisions in Au - Au at RHIC shows a steeper centrality-dependence than the Fermi densities for p - p collisions because the nuclear distribution has a relatively smaller edge diffuseness ($a/R = 0.085$) than the proton one.

The other key quantity of our approach is the impact-parameter dependence of the midrapidity particle multiplicity produced in p - p collisions at $\sqrt{s} = 14$ TeV. Within our framework, we estimate $dN/dy(b)$ via Eqs. (11) and (12). The latter depends on the parton-parton inelastic collision probability dP_{gg}^{inel}/db , Eq. (8), which is shown as a function of scaled impact-parameter (left) and centrality (right) in Fig. 2 for the various proton densities considered in this work. All probabilities are normalised to unity to facilitate the comparison.

4 Eikonal model results for p - p collisions at the LHC

Based on the eikonal model formalism and proton density parametrisations discussed in the previous section, we derive here all basic quantities needed later to estimate the expected amount of elliptic flow in proton-proton collisions at $\sqrt{s} = 14$ TeV: eccentricity, transverse overlap area and particle multiplicity. Again, in order to compare the results for the various proton densities considered in Table 1 (with varying radii R), we present our results as a function of the dimensionless *scaled* impact-parameter $b/(2R)$ and centrality $C = b^2/(4R^2)$, see Appendix I.

Eccentricity: Figure 3 shows the computed eccentricity in p - p at $\sqrt{s} = 14$ TeV as a function of the scaled impact-parameter (left) and centrality (right) of the collision. The eccentricity is increasingly large and positive for the hard-sphere parton density (up to $\varepsilon = 1$ for $b = 2R$) and increasingly negative (down to $\varepsilon = -0.4$ for $b \approx 2R$) for the exponential spatial density. For the Fermi distributions with diffuse edges, the eccentricity is small ($\varepsilon \lesssim 0.1$) and changes its sign for very large impact parameters. The larger the ratio of diffuseness-to-radius ($a/R = 0.28, 0.2$, and 0.0085 for the Fermi-II, Fermi-I, and Fermi-Au-Au respectively) is, the smaller the impact-parameter at which ε changes sign. In any case, the small magnitude of the p - p eccentricities for the Fermi-I (about five times smaller than Fermi-AuAu) and Fermi-II (very close to zero) profiles and the large impact-parameters where the sign change takes place, likely preclude to see any such effect in the elliptic flow data. Also, as aforementioned, it is easy to show that the overlap of two Gaussian distributions for the colliding protons, has zero eccentricity at any impact parameter.

Overlap area: Figure 4 shows the p - p transverse overlap area as a function of scaled impact parameter. The left plot shows the absolute $A_{\perp}(b)$ value, and the right plot presents the overlap-area normalised to the maximum value for a “head-on” collision at zero impact-parameter, $A_{\perp}(b)/A_{\perp}(b=0 \text{ fm})$. The overlap area for central p - p collisions is largest for the Fermi-II density ($A_{\perp} \approx 4 \text{ fm}^2$) and smallest for the exponential distribution ($A_{\perp} \approx 0.6 \text{ fm}^2$). Again, as for the eccentricity, the hard-sphere and exponential distribution have opposite behaviours as a function of centrality: $A_{\perp}(b)$ decreases (increases) for the former (for the latter). On the other hand, there is only a small dependence of the transverse area on impact-parameter for the overlap of two Fermi densities with diffuse edges. Compared to Au-Au, the obtained values of A_{\perp} in p - p collisions, for the Fermi and hard-sphere densities ($A_{\perp} \approx 1 \text{ fm}^2$), are about two orders of magnitude smaller.

Hadron multiplicity: The third ingredient of the incomplete thermalisation model, Eq. (4), is the particle multiplicity per unit rapidity at midrapidity, dN/dy , obtained via Eqs. (11) – (12). The results are shown in Fig. 5 for a value¹⁰ of dN_0/dy

chosen in Eq. (12) so as to reproduce the expected $dN_{MB}/dy = 10$ multiplicity in minimum-bias p - p collisions at the LHC. All proton densities yield similar values of dN/dy in a wide range of centralities C in p - p collisions. The 20% most central collisions result in 2–3 times larger multiplicities than in minimum bias p - p (or Au-Au) collisions for all considered densities. For the comparison Au-Au data, we take $dN/dy = 600$.

As we see from our elliptic-flow “ansatz”, Eq. (4), the v_2 parameter depends on the particle multiplicity but only after normalisation by the size of the system. Figure 6 shows the transverse density multiplicity, namely the ratio of the hadron multiplicity over the transverse overlap area $(dN/dy)/A_{\perp}$, for different forms of the proton matter distribution. We find ratios $(dN/dy)/A_{\perp} \approx 2.5 - 4.5 \text{ mb}^{-1}$ for all distributions in central p - p collisions similar to those found in Au-Au collisions at RHIC except for the dilute Fermi-II density, which features a much lower $(dN/dy)/A_{\perp} \approx 0.5 \text{ mb}^{-1}$ value. Interestingly, although the particle multiplicity is about two orders of magnitude larger in nuclear than in proton collisions, the overlap area is roughly smaller by the same amount (see Fig. 4) and, therefore, the multiplicity density is not very dissimilar in p - p and A-A collisions: $(dN/dy)/A_{\perp} \approx 0.1 - 4.5 \text{ mb}^{-1}$, for all densities within a large interval of centralities.

5 Elliptic flow estimates in p - p collisions at the LHC

From the values of eccentricity ε (Fig. 3), overlap area A_{\perp} (Fig. 4) and hadron multiplicity dN/dy (Fig. 5), as a function of impact-parameter b determined in the previous chapter, and using the Eq. (4) of the incomplete thermalisation model, we can finally obtain the value of the integrated elliptic flow parameter v_2 for each one of the four different proton densities. By construction, $v_2(b)$ will follow the general behaviour of $\varepsilon(b)$. Figure 7 shows the integrated v_2 as a function of transverse particle density expected at midrapidity in p - p collisions at LHC energies. In Fig. 8 we show v_2 versus centrality (left) and versus particle multiplicity (right) normalised by the maximum value in the most central events, $N(C)/N_{max}$, which is a proxy for the reaction centrality C often used experimentally.

Several features are noticeable in both figures. First, the hard-sphere distribution features a maximum value of $v_2 \approx 0.1$, almost twice higher than in Au-Au collisions and much larger than the rest of p - p elliptic flow parameters. The fact that the overlap of two hard-spheres with infinitely sharp edges (see Fig. 3) yields artificially large eccentricities is a well-known fact [2]. We plot this result just to delimit the theoretically maximum amount of v_2 that could be generated within our approach. Second, the maximum v_2 obtained with the Fermi-I profile is about 1.5% and vanishingly small for the dilute Fermi-II distribution. Third, exponential transverse densities for the proton, feature *negative* p - p eccentricities with minimum elliptic flow parameters of the order of -3.5% . A negative integrated v_2 would indicate that the anisotropy of hadron emission is not *in-plane* (as for a positive v_2) but *out-of-plane*, i.e. perpendicular to the reaction plane.

¹⁰ Note that, given our absolute normalisation based on dN_{MB}/dy , the actual N_g and σ_{gg} values do not play practically any role in the final determination of the hadron multiplicity.

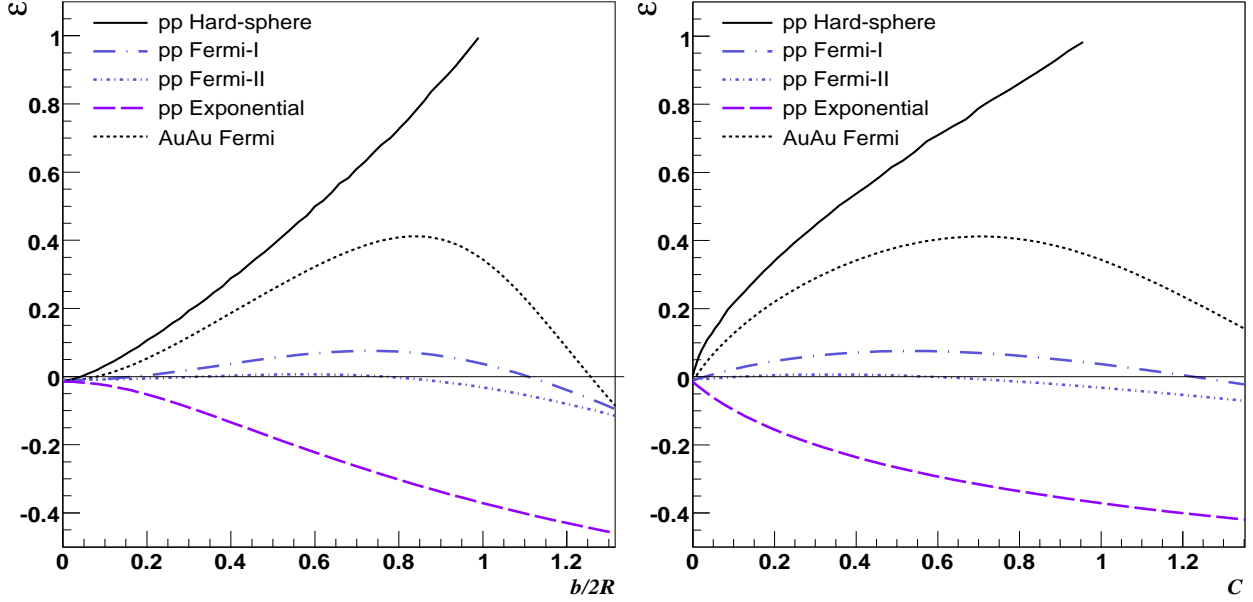


Fig. 3. Eccentricity ϵ in p - p collisions at $\sqrt{s} = 14$ TeV as a function of scaled impact parameter $b/2R$ (left) and centrality C (right) for the different proton density distributions considered in this work (Table 1). For comparison, the results for Au - Au at RHIC energies are shown as a dotted line.

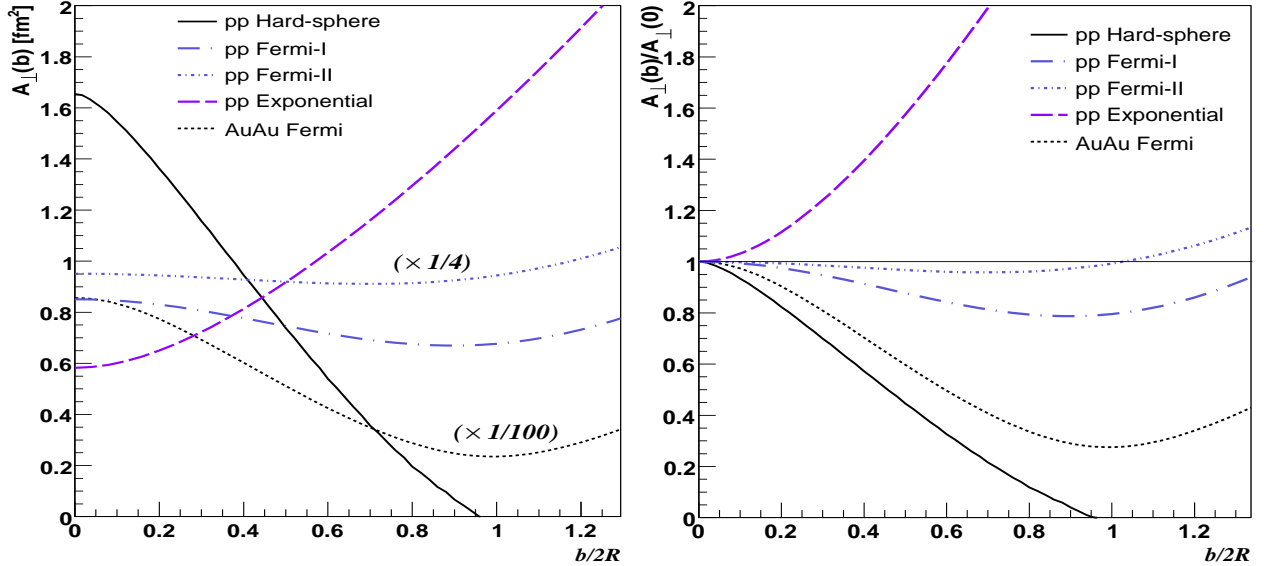


Fig. 4. Effective overlap area A_{\perp} in p - p collisions at $\sqrt{s} = 14$ TeV as a function of scaled impact parameter $b/2R$ for the different proton density distributions considered in this work (Table 1). For comparison, the results for Au - Au at RHIC energies are shown as a dotted line. The left plot shows the absolute value of A_{\perp} (for clarity, the Fermi-II and Au - Au curves are scaled by factors of 1/4 and 1/100 respectively). The right plot shows the area normalised to the value for central collisions, $A_{\perp}(b)/A_{\perp}(b=0 \text{ fm})$.

Setting aside the v_2 obtained with the unrealistic hard-sphere profile, the maximum absolute values of the integrated elliptic flow in p - p collisions in the range 1%–3% are consistent with those obtained in a recent hydrodynamics study [17] – which uses a spatial density based on a parametrisation of the Fourier transform of the proton electromagnetic form-factor [43] – which predicts also $v_2 \lesssim 0.035$ (the maximum value obtained when the produced strongly interacting matter has vanishing viscosity) at 14 TeV. Also percolation models [15] predict integrated

v_2 of the order of 2%–3%. Although small, such v_2 values are comparable to those measured in nucleus-nucleus reactions at c.m. energies $\sqrt{s_{NN}} \approx 5$ GeV at the BNL Alternating Gradient Synchrotron (AGS) [44] or $\sqrt{s_{NN}} \approx 17$ GeV at the CERN Super Proton Synchrotron (SPS) [26] and thus could be in principle measurable.

The experimental measurement of $|v_2|$ signals of maximum magnitude $\mathcal{O}(3\%)$, in p - p collisions at the LHC will be certainly challenging. On the one hand, one will have to deal with

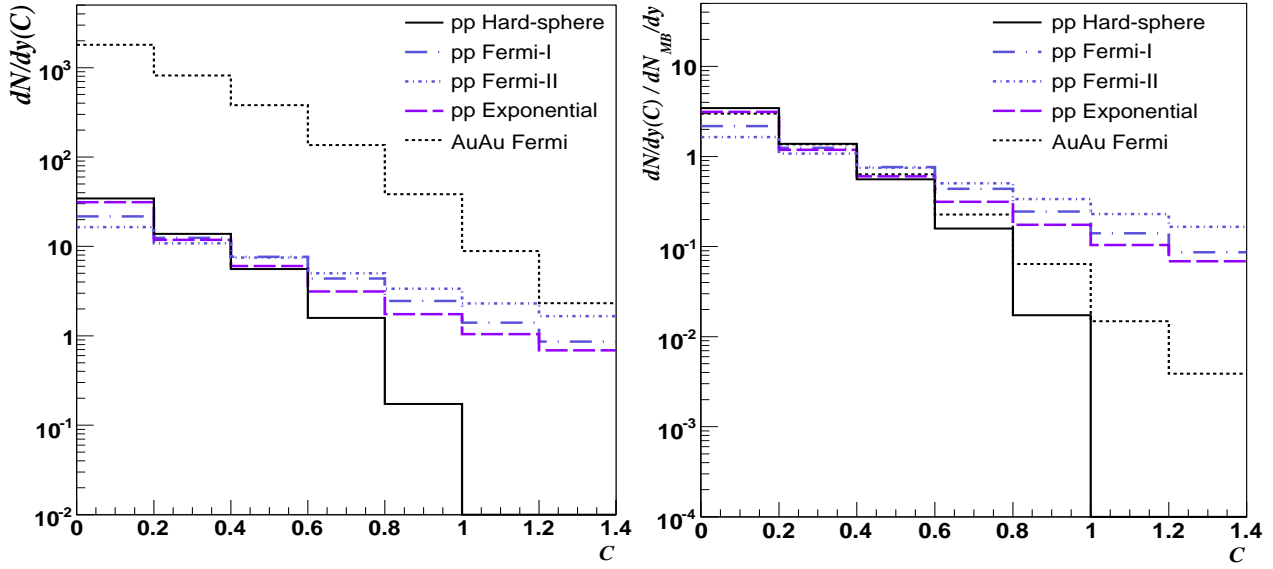


Fig. 5. Absolute (left) and normalised (right) particle multiplicity at midrapidity as a function of centrality C in p - p collisions at $\sqrt{s} = 14$ TeV for the different proton density distributions considered in this work (Table 1). For comparison, the results for Au - Au at RHIC energies are shown as a dotted line.

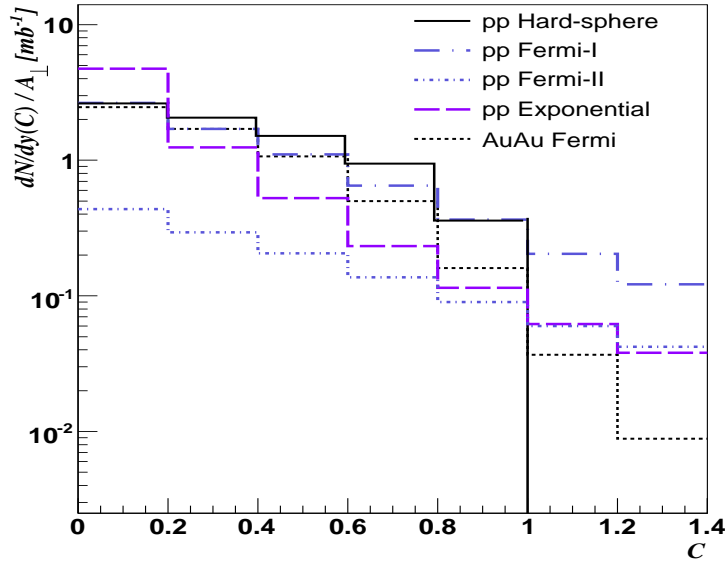


Fig. 6. Particle multiplicity density at $y = 0$ per unit of transverse overlap area A_{\perp} in p - p collisions at $\sqrt{s} = 14$ TeV as a function of centrality C for the different proton density distributions considered in this work (Table 1). For comparison, the results for Au - Au at RHIC energies are shown as a dotted line.

all standard “non-flow” effects – i.e. azimuthal correlations not associated with parton collective rescattering – generated by jets, resonance decays, Hanbury-Brown Twiss (HBT) short-range correlations, or (depending on the technique used to determine v_2) momentum conservation [2]. In particular, the large minijet production cross section at the LHC generates already strong (back-to-back) azimuthal anisotropies [45, 46]. In addition, part of the azimuthal correlations can come, not from final-state rescatterings but from parton correlations in the *initial* state [16, 47]. On the other hand, the relatively small magnitude of the p - p eccentricity and overlap area will result in large

fluctuations of the v_2 parameter even for a same given centrality. Likewise, event-by-event fluctuations on the produced particle multiplicities will also complicate their correlation to the measured v_2 values, as commonly presented in plots like that in Fig. 8 (right). In any case, there exist detailed methods of elliptic flow analyses developed for nuclear collisions [22, 23, 25, 48–51] that can be tested and adapted to p - p collisions at the LHC. We leave for a future paper the detailed study of the experimental feasibility of the measurement. As aforementioned, previous studies in heavy ion collisions at lower energies have clearly demonstrated the possibility to measure v_2 signals with

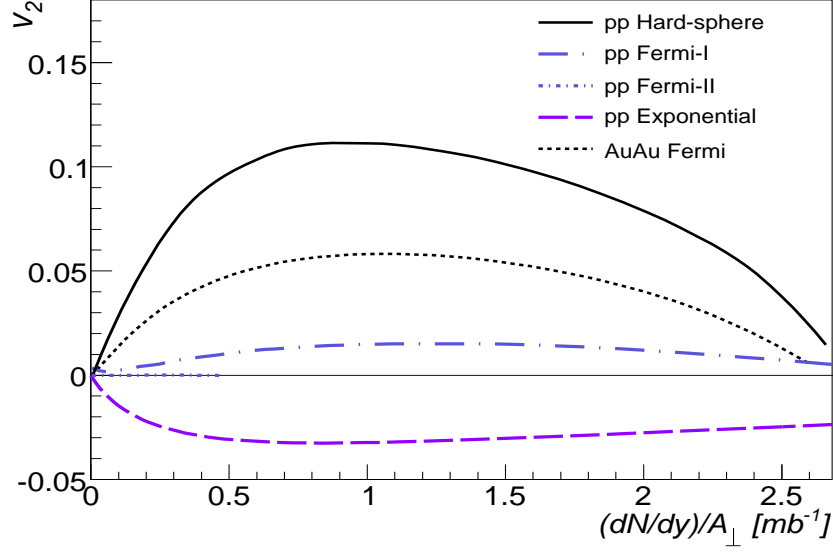


Fig. 7. Integrated elliptic flow v_2 parameter as function of transverse particle multiplicity, $(dN/dy)/A_\perp$, expected at midrapidity in p - p collisions at $\sqrt{s} = 14$ TeV for the different proton density distributions considered in this work (Table 1). For comparison, the Au - Au results are shown as a dotted line.

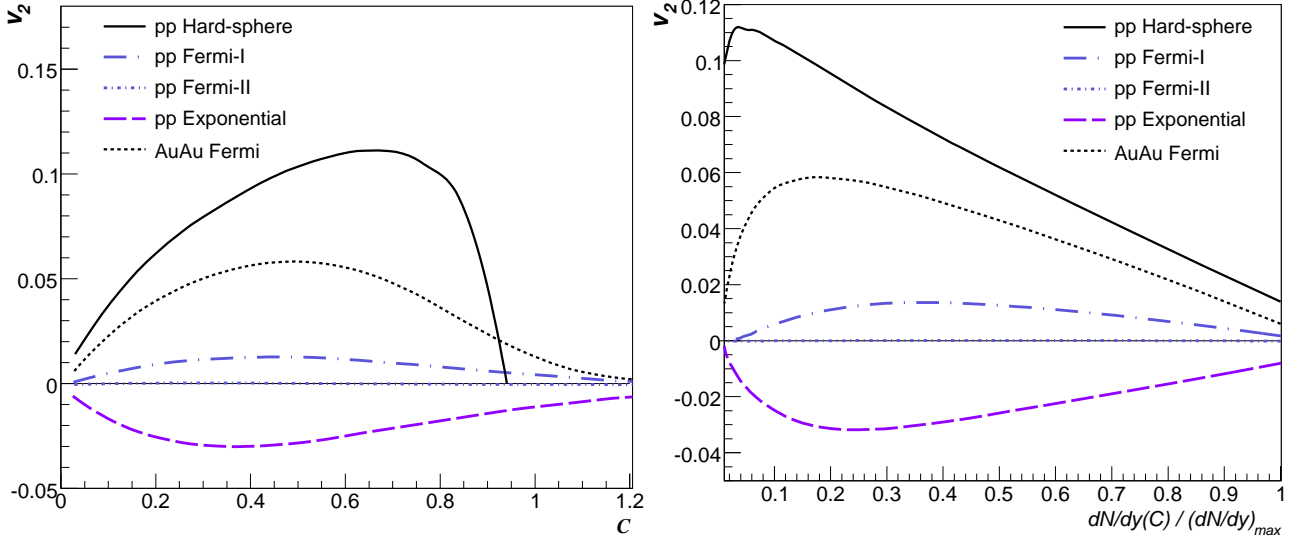


Fig. 8. Integrated elliptic flow v_2 parameter as function of centrality (left panel) and of normalised particle multiplicity (right panel) at midrapidity in p - p collisions at $\sqrt{s} = 14$ TeV for the different proton density distributions considered in this work (Table 1). For comparison, the v_2 for Au - Au at RHIC energies is shown as a dotted line.

absolute magnitudes of order 1%–3% and the ALICE [52], ATLAS [53] and CMS [54] experiments have proven detector capabilities to carry out such measurements.

6 Summary and conclusions

We have studied the possibility to observe a collective expansion signal – in the form of an azimuthal anisotropy of particle production with respect to the reaction plane – due to multiparton interactions in proton-proton collisions at the LHC. Our working assumption has been that any possible azimuthal aniso-

tropy due to collective flow in p - p collisions should follow the same eccentricity, overlap-area and particle multiplicity dependences observed in the strongly interacting matter formed in high-energy heavy ion collisions. Using a simple eikonal model for multiparton scatterings, we have tested various proton density distributions proposed in the literature and obtained the corresponding eccentricities, transverse areas and hadron multiplicities as a function of the impact parameter for p - p collisions at $\sqrt{s} = 14$ TeV. The transverse overlap area A_\perp and the final particle multiplicity at midrapidity dN/dy are about two orders of magnitude smaller in p - p compared to Au - Au collisions. Since the elliptic flow roughly depends on the nor-

malised $(dN/dy)/A_\perp$ ratio, we thus expect any elliptic flow in the p - p systems to be mostly driven by the eccentricity (if any) of the system produced in the collision.

Our first finding is that, popular proton matter profiles such as Gaussian or double-Gaussian result in vanishing p - p eccentricities and, thus, cannot generate any final-state elliptic flow within our approach. Unphysical sharp edge (hard-sphere) profiles result in integrated elliptic flow parameters, $v_2 \approx 10\%$, almost twice larger than found in A - A at RHIC. More realistic Fermi-Dirac distributions with a diffuse proton edge, yield maximum v_2 values of the order of 1.5%. If the Fermi density is too dilute, as in our considered Fermi-II case that takes into account an effective growth of the proton size due to the transverse spread of its partons at high energies, the generated v_2 will be virtually null. Lastly, exponential proton profiles that reproduce the proton charge form-factor (i.e. the spatial distribution of its valence quarks) would result in negative, i.e. out-of-plane, integrated elliptic flows with minimum values of the order of -3% .

All in all, our work demonstrates that the study of hadron anisotropies with respect to the reaction plane in p - p collisions at LHC energies, can provide important information on the proton shape and structure at moderate virtualities $\mathcal{O}(0.7 \text{ GeV})$. Although previous analyses with heavy ions at much lower energies have indeed measured integrated v_2 of a few percents, the experimental extraction of such a signal in p - p collisions will be challenging given the expected large non-flow azimuthal correlations that can mask the signal. Despite these difficulties, the absence or presence of elliptic flow in the data and its dependence on the “centrality” of the collision, will nonetheless put strong constraints on the density profile of the proton at very high energies.

Acknowledgments

We thank Mark Strikman for valuable discussions and comments on a previous version of the paper. This research was supported by Russian Foundation for Basic Research (grants No 08-02-91001 and No 08-02-92496), Grant of President of Russian Federation No 107.2008.2, Dynasty Foundation and Russian Ministry for Education and Science (contracts 01.164.1-2.NB05 and 02.740.11.0244). D.d'E. acknowledges support by the 7th EU Framework Programme (contract FP7-ERG-2008-235071).

Appendix I.

We recall here the basic transformations from impact parameter to centrality for a general two-dimensional probability density $F(b)$ which depends on the impact parameter vector \vec{b} ,

$$\frac{d^2P}{d^2b} = \frac{d^2P}{b db d\phi} = \frac{1}{2\pi} \frac{dP}{b db} = F(b),$$

$$\text{with normalisation } \int d^2b \frac{d^2P}{d^2b} = \int db (2\pi b F(b)) = 1.$$

The corresponding normalised one-dimensional density for the dimensionless impact parameter $b' = b/(2R)$, which we have used in this work to easily compare the results obtained with proton densities with different radii R , is

$$\frac{dP}{db} = 2\pi b F(b) \rightarrow \frac{dP}{db'} = 4\pi R b F(b).$$

For our alternative centrality parameter defined as $C = b^2/(4R^2)$, i.e. $db = 2R^2/b dC$, we have

$$\frac{dP}{dC} = \frac{2R^2}{b} \frac{dP}{db} = \frac{2R^2}{b} 2\pi b F(b) = 4\pi R^2 F(b),$$

$$\text{normalised to } \int dC \frac{dP}{dC} = \int \frac{b}{2R^2} db \frac{2R^2}{b} \frac{dP}{db} = \int db \frac{dP}{db} = 1.$$

Such a definition of C is convenient as it corresponds to a given fraction of the inelastic cross section. Indeed, for two colliding black disks with radii R_1 and R_2 the fraction of the inelastic cross section is

$$\frac{\Delta\sigma_{inel}}{\sigma_{inel}} = \frac{2\pi b \Delta b}{\pi(R_1 + R_2)^2} = \frac{\Delta b^2}{(R_1 + R_2)^2}, \quad b \leq (R_1 + R_2),$$

and thus for two identical disks $R = R_1 = R_2$, we have

$$\frac{\Delta\sigma_{inel}}{\sigma_{inel}} = \Delta \left(\frac{b^2}{4R^2} \right) = \Delta C.$$

The exact definition of centrality c as a fraction of the inelastic cross section is equal to [55]

$$c = \frac{\sigma_{geom}(b_c)}{\sigma_{geom}} = \frac{2\pi \int_0^{b_c} b db (1 - e^{-\sigma_{gg} T_{pp}(b)})}{\sigma_{pp}^{inel}}.$$

In Fig. 9 we compare the exact centrality c to the centrality C used in the present work. Let us consider, as an example of b -to- C transformation, the case of the probability of inelastic parton scatterings, presented in Section 3. Such a distribution, which as a function of impact parameter and centrality reads:

$$\frac{dP_{gg}^{inel}}{db} = 2\pi b F(b) = \frac{2\pi b (1 - e^{-\sigma_{gg} T_{pp}(b)})}{\int d^2b (1 - e^{-\sigma_{gg} T_{pp}(b)})}, \quad \text{and}$$

$$\frac{dP_{gg}^{inel}}{dC} = 4\pi R^2 F(b) = \frac{4\pi R^2 (1 - e^{-\sigma_{gg} T_{pp}(b)})}{\int d^2b (1 - e^{-\sigma_{gg} T_{pp}(b)})}, \quad b = 2R \sqrt{C}$$

is used in our calculations to determine the multiplicity density

$$\frac{d^3N}{dy d^2b}(b) = \frac{dN_{MB}}{dy} \frac{N_{coll,gg}(b) \frac{d^2P_{gg}^{inel}}{d^2b}(b)}{\int d^2b N_{coll,gg}(b) \frac{d^2P_{gg}^{inel}}{d^2b}(b)}.$$

The multiplicity for different centrality bins is:

$$\frac{dN}{dy}(C_k) = \int_{C_k}^{C_k + \Delta C} dC \frac{d^2N}{dy dC}(C).$$

The dimensionless multiplicity and probability in a given impact-parameter and centrality bin are

$$N(b) = \frac{dN}{db} \Delta b, \quad \text{or} \quad N(C) = \frac{dN}{dC} \Delta C,$$

$$P_{gg}^{inel}(b) = \frac{dP_{gg}^{inel}}{db} \Delta b, \quad \text{or} \quad P_{gg}^{inel}(C) = \frac{dP_{gg}^{inel}}{dC} \Delta C.$$

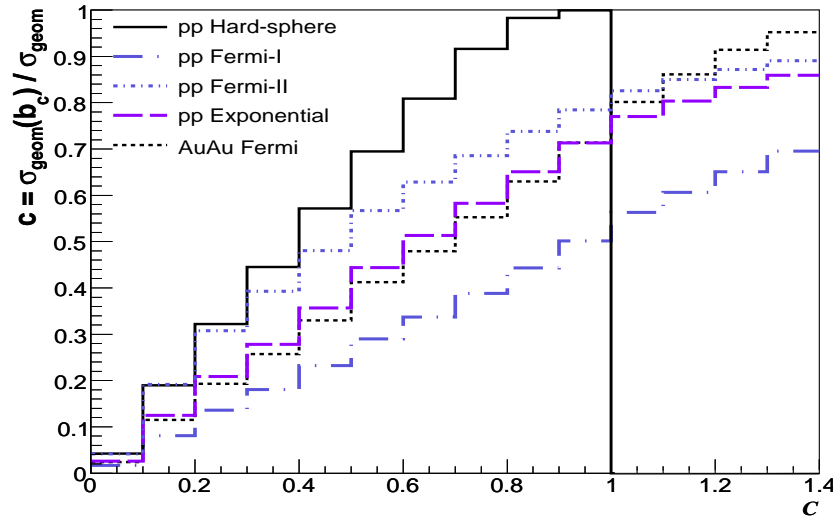


Fig. 9. Comparison of the exact centrality c , Eq. (21), to the centrality $C = b^2/(4R^2)$ used in the present work.

References

1. I. Arsene *et al.* [BRAHMS Collab.], Nucl. Phys. A **757** (2005) 1;
2. B. B. Back *et al.* [PHOBOS Collab.], Nucl. Phys. A **757** (2005) 28;
3. J. Adams *et al.* [STAR Collab.], Nucl. Phys. A **757** (2005) 102;
4. K. Adcox *et al.* [PHENIX Collab.], Nucl. Phys. A **757** (2005) 184
5. S. A. Voloshin, A. M. Poskanzer and R. Snellings, arXiv:0809.2949 [nucl-ex].
6. L. Frankfurt, M. Strikman and C. Weiss, Ann. Rev. Nucl. Part. Sci. **55** (2005) 403.
7. F. Gelis, T. Lappi and R. Venugopalan, Int. J. Mod. Phys. E **16** (2007) 2595.
8. C. Goebel, F. Halzen and D.M. Scott, Phys. Rev. **D22** (1980) 2789;
9. N. Paver and D. Treleani, Nuovo Cimento **A70**, (1982) 215;
10. B. Humpert, Phys. Lett. **B131** (1983) 461 (1983); B. Humpert and R. Odorico, Phys. Lett. **154B** (1985) 211;
11. T. Sjostrand and M. Van Zijl, Phys. Rev. **D36** (1987) 2019.
12. T. Alexopoulos *et al.*, Phys. Lett. B **435** (1998) 453.
13. F. Abe *et al.* [CDF Collab.], Phys. Rev. D **47** (1993) 4857.
14. F. Abe *et al.* [CDF Collab.], Phys. Rev. D **56** (1997) 3811.
15. F. Abe *et al.* [CDF Collab.], Phys. Rev. Lett. **79** (1997) 584.
16. T. Sjostrand and P. Z. Skands, JHEP **0403** (2004) 053
17. J. M. Butterworth, J. R. Forshaw and M. H. Seymour, Z. Phys. C **72** (1996) 637;
18. M. Bahr, S. Gieseke and M. H. Seymour, JHEP **0807** (2008) 076
19. G. I. Veres *et al.* [PHOBOS Collab.], arXiv:0806.2803 [nucl-ex].
20. A. Adare *et al.* [PHENIX Collab.], Phys. Rev. Lett. **98** (2007) 162301
21. H. J. Drescher and M. Strikman, arXiv:0712.3209 [hep-ph].
22. L. Cunqueiro, J. Dias de Deus and C. Pajares, arXiv:0806.0523 [hep-ph];
23. I. Bautista, L. Cunqueiro, J. D. de Deus and C. Pajares, arXiv:0905.3058 [hep-ph].
24. B. Z. Kopeliovich, A. H. Rezaeian and I. Schmidt, Phys. Rev. D **78** (2008) 114009
25. M. Luzum and P. Romatschke, arXiv:0901.4588 [nucl-th].
26. K. H. Ackermann *et al.* [STAR Collab.], Phys. Rev. Lett. **86** (2001) 402
27. K. Adcox *et al.* [PHENIX Collab.], Phys. Rev. Lett. **89** (2002) 212301
28. P. F. Kolb, J. Sollfrank and U. W. Heinz, Phys. Rev. C **62** (2000) 054909
29. D. Teaney, J. Lauret and E. V. Shuryak, arXiv:nucl-th/0110037.
30. J. Y. Ollitrault, Phys. Rev. D **46** (1992) 229.
31. S. Voloshin and Y. Zhang, Z. Phys. C **70** (1996) 665.
32. H. Heiselberg and A. M. Levy, Phys. Rev. C **59** (1999) 2716.
33. S. A. Voloshin and A. M. Poskanzer, Phys. Lett. B **474** (2000) 27.
34. C. Alt *et al.* [NA49 Collab.], Phys. Rev. C **68** (2003) 034903.
35. M. L. Miller, K. Reygers, S. J. Sanders and P. Steinberg, Ann. Rev. Nucl. Part. Sci. **57** (2007) 205
36. C.W. deJager, H. deVries, and C. deVries, Atomic Data and Nuclear Data Tables **14** (1974) 485.
37. R. S. Bhalerao, J. P. Blaizot, N. Borghini and J. Y. Ollitrault, Phys. Lett. B **627** (2005) 49.
38. H. J. Drescher, A. Dumitru, C. Gombeaud and J. Y. Ollitrault, Phys. Rev. C **76** (2007) 024905.
39. C. Gombeaud and J. Y. Ollitrault, Phys. Rev. C **77** (2008) 054904
40. A. Adil, H. J. Drescher, A. Dumitru, A. Hayashigaki and Y. Nara, Phys. Rev. C **74** (2006) 044905.
41. M. Luzum and P. Romatschke, Phys. Rev. C **78** (2008) 034915 [Erratum-ibid. C **79** (2009) 039903]
42. P. F. Kolb and U. W. Heinz, in "Quark gluon plasma 3", World Sci., Singapore; arXiv:nucl-th/0305084.
43. R. Engel, Z. Phys. C **66** (1995) 203.
44. L. Frankfurt, M. Strikman, C. Weiss and M. Zhalov, Czech. J. Phys. **55** (2005) B675
45. R. Hofstadter, Rev. Mod. Phys. **28** (1956) 214.
46. C. Diaconu, Proceeds. DIS2007, Munich, Germany, 16-20 Apr 2007.
47. L. Frankfurt, M. Strikman and C. Weiss, Phys. Rev. D **69** (2004) 114010.
48. M. M. Block and R. N. Cahn, Rev. Mod. Phys. **57** (1985) 563.
49. M. M. Islam, R. J. Luddy and A. V. Prokudin, Mod. Phys. Lett. A **18** (2003) 743.
50. I. Sick, Phys. Lett. B **576** (2003) 62
51. G. A. Miller, Phys. Rev. Lett. **99** (2007) 112001
52. J. Barrette *et al.* [E877 Collab.], Phys. Rev. C **55** (1997) 1420 [Erratum-ibid. C **56** (1997) 2336]
53. I. P. Lokhtin, L. I. Sarycheva and A. M. Snigirev, Eur. Phys. J. C **30** (2003) 103
54. I.P. Lokhtin, L.I. Sarycheva, A.M. Snigirev, Phys. Atom. Nucl. **66** (2003) 2199.

- 47. K. G. Boreskov, A. B. Kaidalov and O. V. Kancheli, Eur. Phys. J. C **58** (2008) 445
- 48. H. Sorge, Phys. Rev. Lett. **82** (1999) 2048.
- 49. A. M. Poskanzer and S. A. Voloshin, Phys. Rev. C **58** (1998) 1671.
- 50. C. N. Yang and T. D. Lee, Phys. Rev. **87** (1952) 404.
- 51. G. Kh. Eyyubova *et al.*, Phys. Atom. Nucl. **71** (2008) 2142; CERN CMS CR 2008/022 (2008).
- 52. B. Alessandro *et al.* [ALICE Collab.], J. Phys. G **32** (2006) 1295.
- 53. P. Steinberg [ATLAS Collab.], J. Phys. G **34** (2007) S527.
- 54. D. d'Enterria (ed.) *et al.* [CMS Collab.], J. Phys. G **34** (2007) 2307.
- 55. R. Vogt, "Ultrarelativistic Heavy-Ion Collisions", Elsevier Science, Amsterdam, 2007.